Thermal behavior and mechanical properties of Y_2SiO_5 environmental barrier coatings after isothermal heat treatment

Byung-Koog Jang, Fan-Jie Feng, Kee-Sung Lee, Eugenio Garcia, Andrés Nistal, Nobuo Nagashima, Seongwon Kim, Yoon-Suk Oh, Hyung-Tae Kim

PII: S0257-8972(16)31098-2
DOI: doi:10.1016/j.surfcoat.2016.09.088
Reference: SCT 21746

To appear in: *Surface & Coatings Technology*

Received date: 18 March 2016
Revised date: 19 August 2016
Accepted date: 22 September 2016

Please cite this article as: Byung-Koog Jang, Fan-Jie Feng, Kee-Sung Lee, Eugenio Garcia, Andrés Nistal, Nobuo Nagashima, Seongwon Kim, Yoon-Suk Oh, Hyung-Tae Kim, Thermal behavior and mechanical properties of Y_2SiO_5 environmental barrier coatings after isothermal heat treatment, *Surface & Coatings Technology* (2016), doi:10.1016/j.surfcoat.2016.09.088

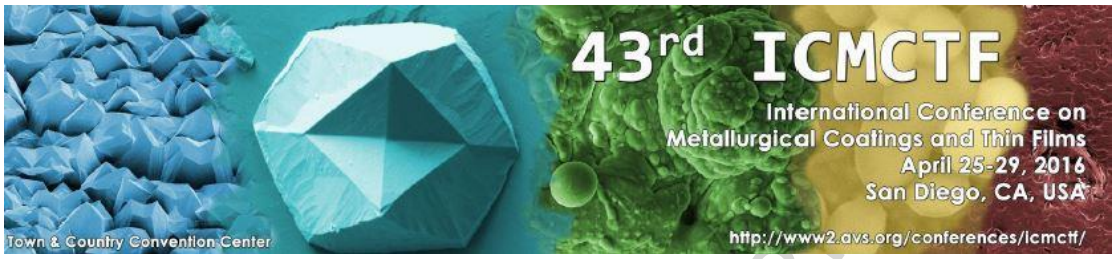

MANUSCRIPT REPORT FORM

PAPER NUMBER (if known)； Abstract #742 (session number # A2-3-4)
TITLE OF PAPER: Thermal behavior and mechanical properties of Y_2SiO_5 environmental barrier coatings after isothermal heat treatment

PRESENTING AUTHOR: Byung-Koog Jang
FULL MAILING ADDRESS: Research Center for Structural Materials,
National Institute for Materials Science (NIMS)
1-2-1 Sengen, Tsukuba, Ibaraki 305-0047, Japan
TELEPHONE: +81-29-859-2453(direct)
FAX: +81-29-859-2401
E-MAIL: JANG.Byungkoog@nims.go.jp

CORRESPONDING AUTHOR: Byung-Koog Jang
FULL MAILING ADDRESS: Research Center for Structural Materials,
National Institute for Materials Science (NIMS)
1-2-1 Sengen, Tsukuba, Ibaraki 305-0047, Japan
TELEPHONE: +81-29-859-2453(direct)
FAX: +81-29-859-2401
E-MAIL: JANG.Byungkoog@nims.go.jp

Thermal behavior and mechanical properties of Y_2SiO_5 environmental barrier coatings after isothermal heat treatment

Byung-Koog Jang[1),*], Fan-Jie Feng[2)], Kee-Sung Lee[2)], Eugenio Garcia[3)], Andrés Nistal[3)], Nobuo Nagashima[1)], Seongwon Kim[4)], Yoon-Suk Oh[4)] and Hyung-Tae Kim[4)]

[1)]National Institute for Materials Science, 1-2-1 Sengen, Tsukuba, Ibaraki 305-0047, Japan

[2)]School of Mechanical Systems Engineering, Kookmin University, 77, Jeongneung-ro, Seongbuk-gu, Seoul 136-702, Korea

[3)]Institute of Ceramics and Glass, ICV—CSIC, Kelsen 5, 28049 Madrid, Spain

[4)]Korea Institute of Ceramic Engineering and Technology, 3321 Gyeongchung Rd, Sindun-Myeon, Icheon 17303, Korea

* Corresponding author:

Tel.: +81-29-859-2453; Fax: + 81-29-859-2401

E-mail address: JANG.Byungkoog@nims.go.jp (B.K. Jang)

Abstract

Y_2SiO_5 coatings are deposited by a flame-spray technique as protection layer on SiC substrates to prevent oxidation and steam corrosion. In this research, Y_2SiO_5 coatings were isothermally heat treated at different temperatures and different exposure times in a laboratory environment. The thermal behaviors such as phase transformation, microstructural change and thermally grown oxide (TGO) formation have been examined by XRD, SEM, and EDS analysis. Different modes of TGO growth behavior were found at different temperatures. In addition, the mechanical properties were evaluated by a Martens hardness tester. The results show that the change of microstructure and composition is not too critical, but higher temperatures and longer heating times do lead to the formation of Y_2SiO_5 crystalline phases and a β-Y_2O_3 phase. Thus, the isothermal heat treatment improves the hardness and elastic modulus of Y_2SiO_5 coatings.

Keywords: Environmental barrier coatings, Y2SiO5, Isothermal heat treatment, Thermal growth oxide, Mechanical properties.

1. Introduction

As a high-efficiency energy conversion system, the gas turbine plays an increasingly important role in various applications, such as stationary power generators and aircraft jet engines[1)]. Operation temperature is one of the main factors that must be taken into account in order to evaluate a turbine system, and it is generally known that combustion efficiency increases with increasing operation temperature. Recently, a 1600 °C-class, high-efficiency J-type gas turbine has been developed. Relative to the 1300 °C-class E-type gas turbine, the J-type can reach a combined cycle efficiency as high as 61.5%[2)]. Generally, the upper limit of operating temperature for the hot gas path parts (HGPPs) of last-generation gas turbine materials, i.e., thermal barrier coatings (TBCs) plus super alloys, is about 1300 °C. Hence, these materials are not able to fulfill the requirements of the new-generation gas turbine hot parts.

Therefore, a new advanced material is required[3-4)]. Because of their excellent high-temperature mechanical properties (e.g., retention of high-temperature strength and toughness up to 1600 °C), non-oxygen silicon-based ceramics such as silicon nitride (Si_3N_4) and silicon carbide (SiC) are of interest as candidate materials for the HGPPs of new-generation gas turbines. However, since it is prone to hot-corrosion in thermally extreme environments, the development of environmental barrier coatings (EBCs) is mandatory[5-8)]. In addition to high melting point and low thermal conductivity, ideal EBC materials should have low oxygen diffusion, favorable

chemical stability, thermodynamic compatibility with the substrate, and a coefficient of thermal expansion (CTE) closely matched to that of the substrate[9-11]. Based on the above criteria, mullite ($3Al_2O_3 \cdot 2SiO_2$) has been investigated as a first generation EBC material[12]. Single-layer mullite top coatings exhibit low oxygen diffusion and a perfect CTE match with non-oxygen silicon-based ceramic substrates. However, the lack of thermal shock resistance of mullite top coatings will cause microcracks at service temperatures above 1000ºC, leading to degradation such as premature delamination from the substrate[13]. More recently, a multi-layer EBC structure including a BaO-SrO-Al_2O_3-SiO_2 (BSAS) top coating layer and a mullite intermediate layer has been developed[14]. Unfortunately, the problems in terms of CTE mismatch that occur in multi-layer structures are normally more serious than in single-layer EBC structures[15]. Hence, Lee *et al.* have proposed a new single-layer EBC structure containing rare earth silicate (RE-silicate) materials. Usually, rare earth silicate exists as RE-monosilicate (RE_2SiO_5) or RE-disilicate (RE_2Si2O_7). After Ogura *et. al*. first proposed yttrium monosilicate (Y_2SiO_5) as a potential EBC material for protection of SiC substrates from oxidation and steam corrosion, various additional studies have been reported[16]. The thermal and mechanical properties of single-phase Y_2SiO_5 bulk ceramic material that were observed by Sun *et. al.* indicated that Y_2SiO_5 bulk material has a much lower thermal conductivity than other commonly used EBC materials. In addition, low shear deformation resistance and good machinability have also been reported[17]. Compared with Y_2SiO_5 bulk material, Y_2SiO_5 ceramic coatings exhibit a range of characteristics caused by various factors such as different coating techniques,

parameters, and feedstock. The two most common coating techniques, atmospheric plasma spray (APS) and electron beam physical vapor deposition (EB-PVD) have been extensively employed to create Y_2SiO_5 ceramic coatings; however, Y_2SiO_5 coatings by other coating techniques are rarely seen. Furthermore, investigations of the influence of isothermal heat treatment on these coatings have not been conducted. In previous work, a more cost-effective, more convenient variation of the flame-spray coating technique has been employed to create Y2SiO5 EBCs top coatings using flame spheroidization (FS) feedstock[18]. The results showed that, compared with APS coating technique using spray-dried feedstock, the coating surface morphology showed melted splats but not all of them were fully flattened. In addition, some entrapped porosity in the flattened zone was observed[19].

In the present study, the isothermal heat treatment of Y_2SiO_5 EBC top coatings produced by flame spray using powder feedstock has been performed at 1180 °C and 1480 °C for various exposure times. The influence of different heat treatment temperatures and holding times on the coating microstructure, crystallization and thermally grown oxide (TGO) phenomena have been investigated by scanning electron microscopy (SEM), X-ray diffraction (XRD), and energy-dispersive X-ray spectroscopy (EDS) analysis, respectively. Moreover, the influence of crystallization on the mechanical properties such as Martens hardness and Young's modulus were also investigated.

2. Experimental procedures

2.1. Sample preparation and isothermal heat treatment

The SiC substrate was prepared by powder processing and spark-plasma sintering (SPS). The SiC powder was put into a graphite mold with a diameter of 30 mm. The mold was placed in the spark plasma apparatus (Syntex, Inc. Co., Japan) and the temperature was raised to 1400–1600 °C in a vacuum of 10^{-2} Pa. The sintering was conducted under 60 MPa of pressure.

In our previous work, a Y_2SiO_5 top coating was deposited on a silicon bond coat as an EBC on a silicon carbide substrate by a flame-spray coating technique which used an oxygen-acetylene gun (model CastoDyn DS 8000, Eutectic Castolin, Madrid, Spain). The torch input power was 28 kW, the acetylene-oxygen volumetric flow ratio was that of the stoichiometric mixture and the oxygen and acetylene pressures were 4×10^5 and 7×10^4 Pa, respectively. The stand-off distance was the same employed for 15 cm. The details of the coating process are described elsewhere[19-20].

In the present study, the as-sprayed samples (including coatings and substrate) were cut with a diamond saw into 30 mm × 30 mm specimens with a thickness of 5 mm. After ultrasonic cleaning with acetone and ethanol, the isothermal heat treatment was carried out in a laboratory environment using a furnace with a maximum temperature capability of 1700 °C (KBF314N, Koyo Thermo Systems Co. Ltd., Japan). The isothermal heat treatments were performed at 1180 °C and 1480 °C with holding

times of 1, 10, 50, and 100 h. The heating rate was 5 °C per minute; after the heat treatment, the treated samples were naturally cooled back down to room temperature.

2.2. Characterization

Phase analyses were performed by XRD (D/MAX-2200, Rigaku Co. Ltd., Japan) at a wavelength of 1.5406Å, with Cu *Kα* radiation at a scan rate of 3° per minute over the 2θ range of 20°–80°.

Microstructure observation and analysis were carried out by means of SEM (JSM-6010F, JEOL Co., Japan) with an acceleration voltage of 15 kV and current of 20 μA. EDS was employed to determine the element species, distribution and their contents with an acceleration voltage of 20 kV and working distance of 10 mm.

In order to obtain the hardness and Young's modulus of specimens experimentally, a Martens hardness test was performed on the cross-section of the Y_2SiO_5 top-coating using an UltraMicro Hardness Tester (DUH-211, Shinmadzu Co. Ltd., Japan) at room temperature. The hardness and Young's modulus were derived from load-displacement curves as a function of indentation depth during the load–unload process in accordance with the standard method of ISO 14577-1 (Annex A) as shown in Fig.1. The cross section of each sample was polished up to mirror smoothness using diamond suspensions of 15, 9, 6, 3, 1, and 0.5 μm in sequence. The measurements were carried out with a 115° triangular pyramid indenter, which applied 100 mN of constant test force with a loading time of 10 s and an unloading time of 20 s. To acquire the average values, at least 10 indents were measured; to

maintain accuracy, the center area of the top coating of each sample was chosen as the test region through the simultaneous observation by optical microscopy. In addition, optical microscopy is also used to avoid the pores and un-melted feedstock that inevitably exist in ceramic coatings. Finally, the Martens hardness (HM) was obtained from the following equation[21]:

$$HM_{115} = 1000\ F / 26.43 \times h^2$$

where F is the maximum force and h is the depth corresponding to the maximum force, the 26.34 is projected contact area which is a constant that applies when using a 115° triangular pyramid indenter.

In this study, the indentation elastic modulus (E_{it}) was regarded as Young's modulus of the coatings, which can be proposed as the following equation[21,22]:

$$\frac{1}{Er} = \frac{(1-Vi^2)}{Ei} + \frac{(1-Vs^2)}{Eit}$$

where E_i is the Young's modulus of the indenter (1141 Gpa) and ν_i is Poisson's ratio for the indenter (0.07), the ν_s is defined as Poisson's ratio for specimen (0.31) [23], moreover, the converted elastic modulus based on the indentation contact E_r can be extracted from the following relation [22,24]:

$$E_r = \frac{1}{2}\sqrt{\frac{\pi}{A}}\frac{dp}{dh}$$

where A is the indenter contact area, dp is the load increment and dh is the increment of the indentation depth in the range of 60–95% of maximum load for unload after loading.

3. Results and discussion

3.1. Microstructure and phase analysis of the as-sprayed sample

The cross-sectional microstructure and element-mapping results for an as-sprayed sample are shown in Fig.2. Y_2SiO_5 powder feedstock (FS) has been deposited on the silicon bond-coating by a flame spray coating technique before EBCs coating on the polycrystalline SiC substrate. Both the top layer and the bond-coating layer possess a homogeneous and integrated microstructure. The detailed microstructure is shown in Fig.2 (a); the surface morphology of the as-sprayed Y_2SiO_5 top coating is platy and dense. The coating layer contains micro-sized internal cracks. Vertical cracks are also found in the top coating; some of them appear to have propagated into and through the entire top coating. However, no visible gaps were found in the interface between the top and bond coating, which demonstrates the good chemical compatibility of yttrium monosilicate with silicon materials.

The EDS mapping results of a cross-section of the as-sprayed sample are shown in Fig.2. The elements yttrium and oxygen in Fig.2 (b) and (c), are only present in the outermost coating, which indicates that neither of these elements has moved or migrated across the interface between the top coating and the bond coating. This is a very important piece of information that will help us to interpret observations of the TGO growth phenomenon during subsequent isothermal heat treatment processes. In

addition, while the silicon is evenly distributed within each layer, the Si concentration of each layer are quite different from one another as shown in Fig.2 (d).

XRD patterns of the as-sprayed top coating and detail patterns in the range of 30°~34° are shown in Fig.3 (a) and (b). The main constituent of the as-sprayed coatings is the cubic Y_2O_3 phase (PDF #43-0661), which is a fluorite-type high-temperature polymorph of α-Y_2O_3 (space-group Fm3). Due to the rough coating surface morphology that was produced during the flame spray coating process, it enhances the intensities of XRD reflections. Due to present extremely high peak before 30 degree, therefore, the relatively weak peaks indicating minor phases may be neglected. The patterns in the range of 30°–34° are magnified in Fig.3 (b), showing that the monoclinic structure of the Y_2SiO_5 phase (PDF #41-0004) is present as a minor phase. It is noteworthy that free standing silica was not detectable in the as-sprayed top coatings, suggesting that it is present in a glassy state. In addition, because of the rapid solidification, no phase transformations occurred during the flame-spray processing, and the crystalline phases observed in the coating are very similar to those present in the feedstock; this is consistent with the previous work by Eugenio *et al.*[19-20].

3.2. Thermal behavior by isothermal heat treatment

The XRD patterns of Y_2SiO_5 coatings after isothermal heat treatment at 1180 °C for different exposure times are compiled in Fig.4. Even though no crystallinity is

indicated by the XRD patterns from the sample that was isothermal heat-treated for 1 h, the large discrepancy in terms of intensity of the XRD patterns between it and the as-sprayed sample implies that the rough surface morphologies of the top coatings have been changed. In addition, crystallization definitely occurred after an exposure time of 10 h. Compared with the as-sprayed coatings, two new phases are generated, namely cubic structure α-Y_2O_3 (PDF #73-1334, space-group La3) and monoclinic structure Y_2SiO_5 (PDF #36-1476). The new first peak in the XRD patterns, α-Y_2O_3, is believed to have crystallized from the existing amorphous Y_2O_3 that was produced during the flame-spray coating process. Also, another new phase in terms of monoclinic Y_2SiO_5 can be considered as generation according to via equation (1), which can attribute to non-fully synthetic feedstock.

$$Y_2O_3 + SiO_2 = Y_2SiO_5 \quad (1)$$

In addition, nearly identical XRD patterns are displayed in Fig.4 (c), (d), (e); this implies that at temperature of 1180 °C, the phase state of the top coating will stabilize after 10 h of heat treatment, and present mixed phases of cubic structure α-Y_2O_3 and monoclinic Y_2SiO_5. On the other hand, when the isothermal temperature was increased to 1480 °C, the emergence of crystallinity occurred after only 1 h of heat treatment as shown in Fig.5 (b); this result indicates that a higher isothermal temperature can accelerate the crystallization rate of top coatings. Moreover, after 10 h of heat treatment at 1480 °C, a new m-Y_2O_3 phase (monoclinic Y_2O_3 phase)was found in the XRD patterns as shown in Fig.5 (c), (d), (e). It is worth noting that the

existence of this new phase can improve the mechanical properties of the entire top coating; this will be discussed subsequently.

The surface morphology of the coatings after isothermal heat treatment at 1180 °C is shown in Fig.6. The morphology exhibits melted and flattened splats, and the flat structure of the splats implies well bonded and dense coatings. Macroscopic networks of evenly spaced cracks were exposed in SEM images (a) and (b) at low magnification. Certainly, they also exist in (c) and (d), but the widths of the micro cracks are so narrow that they have to be observed utilizing a high magnification SEM image (g) and (h); this indicates that the width of the cracks decreased as the heat-treatment times increased. This phenomenon can be attributed to volume changes, which were produced by grain growth in the top coatings after isothermal heat treatment. As shown in the high magnification SEM image, slight grain growth was observed in Fig.6 (f) after 10 h of heat treatment, and holistic crystallization occurred after 50 h, showing good agreement with the analysis above.

A cross sectional SEM image of an isothermal heat-treated sample after 100 h of heat treatment at 1180 °C is shown in Fig.7 (a). The TGO layer can be clearly observed at the interface between the top coating and bond coating. To determine the composition of the TGO (the darkest area, average thickness: 20μm), an EDS line scan was performed across the TGO zone. Fig.7 (b) illustrates the distribution trends of yttrium, silicon, and oxygen, indicating that yttrium did not diffuse out of the top coating. The atomic percentage of yttrium has dropped to zero before the line scan reaches the TGO boundary, but the atomic percentage of oxygen does not decrease

along with the reduction in yttrium. Moreover, a measurable amount of oxygen element extends all the way to the silicon bond coating area. According to the analysis of Fig.7 (b), this may imply that the oxygen element present only at the top coating reacts with Si. We conclude that the TGO is composed of silica that comes from the reaction of silicon and oxygen. Based on the above analysis, the silica composition of the TGO layer was influenced by the temperature and/or the time of the isothermal heat treatment, as shown in Fig. 7. The distribution of oxygen affecting the TGO thickness was analyzed by EDS mapping as a function of the isothermal heating temperature and time. The images of Fig.8 (a), (b), (c), and (d) were recorded after isothermal heat treatment times of 1, 10, 50, and 100 h, respectively, at a temperature of 1180 °C, and TGO was detected after 50 h of annealing. However, when the temperature was increased to 1480 °C, the growth phenomenon was observed after only 10 h of annealing, as shown Fig.8 (f). In addition, the thickness of the TGO increased as a function of the heat treatment time in both the 1180 °C case and the 1480 °C case. The difference is that the samples which were heat treated at the relatively low temperature of 1180 °C exhibit less growth than those treated at the relatively high temperature of 1480 °C. Moreover, the TGO growth behavior at 1180 °C exhibits uniform growth along the interface of the top and bond coatings, whereas more aggressive TGO growth behavior occurred in the samples that were heated to 1480 °C, as shown in Fig.8 (g) and (h). The figures show where the TGO has penetrated the bond coatings and has grown from the top coating to the substructure.

3.3. Mechanical properties

The influence of temperature and/or heat treatment times on the mechanical properties are reflected in the average values of Martens hardness on the cross-sectional top coatings as shown in Fig. 9. In the case of the as-sprayed sample, the coatings exhibit a Martens hardness of 4.8±0.1 GPa. However, after isothermal heat treatment at either 1180 °C or 1480 °C, the Martens hardness exhibits a steadily rising trend with increasing heat treatment times. In addition, the coatings treated at1480 °C always exhibit higher hardness values than those treated at 1180 °C. This is attributed to the fact that high temperature can accelerate crystallization growth and the formation of the monoclinic β-Y_2O_3 phase. According to the literature[25], β-Y_2O_3 grains (i) are much smaller than α-Y_2O, and (ii) form characteristic lamellae exhibiting a striking similarity to features observed for martensitic transformation. The above analyses show good agreement with Fig.9; thus, these coatings exhibit a trend of improved mechanical properties that increase not only with heat treatment times, but also with temperature.

Another important mechanical property, Young's modulus, was also measured. The influence of temperature and/or heat treatment times on the Young's modulus of the coatings after isothermal heat treatment at either 1180 °C or 1480 °C is shown in Fig.10. The as-sprayed sample shows a Young's modulus value of nearly 127 GPa. However, after isothermal heat treatment at 1180 °C or 1480 °C, The Young's

modulus values show the same tendency as the the Martens hardness that was shown in Fig.9. The result exhibits a steadily rising trend with increasing heat treatment times. Moreover, the Young's modulus of the coatings after heat treatment at 1480 °C is higher than that after heat treatment at 1180 °C. This result can also be attributed to the fact that crystallization phenomena at relatively high temperatures occur faster and more completely than at relatively low temperatures.

4. Conclusions

In this study, the influence of different heat treatment temperatures and holding times on the microstructure, crystallization, and thermally grown oxide behavior of flame-sprayed Y_2SiO_5 coatings were investigated. Moreover, the influence of crystallization on mechanical properties such as Martens hardness was also studied. The main conclusions to be drawn are as follows:

Crystallization occurred during isothermal heat treatment; the phase-composition of the top coatings stabilized after 10 h of heat treatment at 1180 °C, and after 1 h of heat treatment at 1480 °C. In addition, new phases appeared during the heat treatments, namely cubic α-Y_2O_3, monoclinic β-Y_2O_3 and Y_2SiO_5 phases. It is worth noting that monoclinic β-Y_2O_3 can improve the mechanical properties of the entire top coating, as measured by the Martens hardness and Young's modulus.

TGO phenomena were observed by SEM imaging; EDS line scans indicated that the composition of the TGO is silica. Moreover, the TGO growth behavior can be clearly

detected by EDS mapping of the distribution of oxygen. In addition, gentle and uniform TGO growth and some aggressive TGO growth behavior was found during isothermal heat treatment at 1180 °C and 1480 °C, respectively.

Acknowledgements

This work was carried out with financial support from National Institute for Materials Science (NIMS) and Korea Institute of Ceramic Engineering and Technology (KICET).

References

1) V. Karl, H. Nabielek, and J. M. Kendall, Coated Particle Fuel for High Temperature Gas Cooled Reaactors, *Nucl. Eng. Tech.*, 2007 **39** [5], p 603-616

2) K. N. Lee, Current Status of Environmental Barrier Coatings for Si-Based Ceramics, *Surf. Coat. Tech.*, 2000, **1** [7], p 133-134

3) F. J. Feng, H. S. Moon, C. W. Kwak, J. Y. Park and K. S. Lee, Fabrication and Characterization of Environmental Barrier Coatings by Spray Drying and Atmospheric Plasma Spraying for Protecting Silicon Carbide Ceramics. *Journal of the Korean Ceramic Society.*, 2014, **51**[5] P 481-486

4) F. J. Feng, D. H. Lee, J. Y. Park and K. S. Lee, Fabrication and Characterization of Silicate-based Ceramics for Environmental Barrier Coatings. *Journal of the Ceramic Processing Research.* (in press)

5) K. N. Lee, D. S. Fox, and N. P. Bansal, Rare Earth Silicate Environmental Barrier Coatings for SiC/SiC Composites and Si3N4 Ceramics, *J. Eur. Ceram. Soc.*, 2005 **25**, p 1705-1715

6) S. Ramasamy, S. N. Tewari, K. N. Lee, R. T. Bhatt, and D. S. Fox, Slurr y Based Multilayer Environmental Barrier Coatings for Silicon Carbide and Silicon Nitride Ceramics — II. Oxidation Resistance, *Surf. Coat. Tech.*, 201 0 **205**, p 266-270

7) J. Kimmel, N. Miriyala, J. Price, K. More, P. Tortorellib, H. Eatonc, G. Li nseyc, and E. Sun, Evaluation of CFCC Liners with EBC after Field Testin

g in a Gas Turbine, *J. Eur. Ceram Soc.*, 2002 **22**, p 2769-2775

8) M. Aparicio, and A. Duran, Yttrium Silicate Coatings for Oxidation Protecti on of Carbon-Silicate Carbide Composites, *J. Am. Ceram. Soc.*, 2000 **83** [6], p 1351-1355

9) J. R. Price, M. V. Roode, and C. Stala, Ceramic oxide-coated silicon carbi de for high temperature corrosive environments, *Key. Eng. Mater.*, 1992 **72**, [74] p 71-84

10) C. V. Cojocaru, D. Levesque, C. Moreau, and R. S. Lima, Performance of Thermally Sprayed Si/mullite/BSAS Environmental Barrier Coatings Exposed to Thermal Cycling in Water Vapor Environment, *Surf. Coat. Tech.*, 2013 **2 16**, p 215-223

11) J. L. Smialek, R. C. Robinson, E. J. Opila, D. S. Fox, and N. S. Jacobson, SiC and Si3N4 recession due to SiO2 scale volatility under combustor cond itions, *Adv. Compos. Mater.*, 1999 **8**(1), p 33-45

12) S. Ramasamy, S. N. Tewari, K. N. Lee, R. T. Bhatt, and D. S. Fox, EBC Development for Hot-Pressed Y_2O_3/Al_2O_3 doped Silicon Nitride Ceramics, *Mat. Sci. Eng A.,* 2010 **527,** p 5492-5498

13) M. P. Brady, B. L. Armstrong, H. T. Lin, M. J. Lance, K. L. More, L. R. Walker, F. Huang, and M. L. Weaver, Feasibility Assessment of Self-Gradi ng Metallic Bond Coat Alloys for EBCs/TBCs to Protect Si-Based Ceramis, *Scr Mater.,* 2005 **52**, p 393-397

14) K. N. Lee, D. S. Fox, J. I. Eldridge, D. Zhu, R. C. Robinson, and N. P. Bansal, Upper Temperature Limit of Environmental Barrier Coatings Based

on Mullite and BSAS, *J. Am. Ceram. Soc.*, 2003 **86** [8], p 1299-1306

15) B. J. Harder and K. T. Faber, Transformation Kinetics in Plasma-Sprayed Barium- and Strontium-Doped Aluminosilicate (BSAS), *Scr. Mater.*, 2010 **62**, p 282-285

16) A. Abdul-Aziz, and R. T. Bhatt, Modeling of Thermal Residual Stress in E nvironmental Barrier Coated Fiber Reinforced Ceramic Matrix, *J. Compos. Mater*., 2012 **46** [10], p 1211-1218

17) V. Herb, G. Couégnat, and E. Martin, Damage Assessment of Thin SiC/SiC Composite Plates Subjected to Quasi-Static Indentation Loading, *Composite A.*, 2010 **41**, p 1677~1685

18) Z. Q. Sun, J. Y. Wang, M. S. Li and Y. C. Zhou, Mechanical properties a nd damage tolerance of Y2SiO5, *J. Eur. Ceram. Soc.*, 2008 **28**, p 2895–29 01

19) E. Garcia, P. Miranzo, and M. I. Osendi, The Prospect of Y2SiO5-Based Materials as Protective Layer in Environmental Barrier Coatings, *J. Therm. Spray Technol.*, 2013 **22**, p 680-689

20) E. Garcia, J. Mesquita-Guimaraes, P. Miranzo, M. I. Osendi, Y. Wang, R. S. Lima, and C. Moreau, Mullite and Mullite/ZrO_2-7wt.%Y_2O_3 Powders for Thermal Spraying of Environmental barrier coatings, *J. Therm. Spray Tech nol.*, 2010 **19**, p 286-293

21) I.S.O 14577-1. Metallic materials—Instrumented indentation test for hardness and materials parameters. Part 1. Test method. Switzerland: International Or ganization for Standardization, Geneva; 2002.

22) W. C. Oliver and G. M. Pharr, An improved technique for determining hardness and elastic modulus using load and displacement sensing indentation experiments, *J. Mater. Res.*, 1992 **7,** p1564-1583

23) Z. J. Sun *et.al*, Mechanical properties and damage tolerance of Y_2SiO_5, J. *Eur. Ceram. Soc*., 2008 28, p2895-2901

24) B. K. Jang, and H. Matsubara, Influence of Porosity on Hardness and Young's Modules of Nanoporous EB-PVD TBCs by Nanoindentation, *Mater. Lett*., 2005, **59**, p 3462-3466

25) P. Mechnich, and W. Braue, Air plasma-sprayed Y_2O_3 coatings for Al_2O_3/ Al_2O_3 ceramic matrix composites, *J. Eur. Ceram. Soc.,* 2013 **33**,p 2645-2653

Figure captions

Fig.1. A schematic illustration of the load-displacement curve by indentation.

Fig.2. As-sprayed sample (a) SEM image of cross-sectional view and EDS elemental mapping results of (b) Yttrium, (c) Oxygen, and (d) Silicon.

Fig.3. XRD patterns of (a) As-sprayed top-coating and (b) detailed patterns in the range of 30~34 degrees.

Fig.4. XRD patterns on coating surface after isothermal heat treatment at 1180ºC of (a) As-sprayed, (b) 1 h annealing, (c) 10 h annealing, (d) 50 h annealing, and (e) 100 h annealing.

Fig.5. XRD patterns on coating surface after isothermal heat treatment at 1480ºC of (a) As-sprayed, (b) 1 h annealing, (c) 10 h annealing, (d) 50 h annealing, and (e) 100 h annealing.

Fig.6. SEM images of coating surface after isothermal heat treatment at 1180ºC of (a) 1 h annealing, (b) 10 h annealing, (c) 50 h annealing, (d) 100 h annealing with low magnification and (e), (f), (g), (h) with high magnification, respectively.

Fig.7. EDS line scan across the TGO deposition zone; (a) location of the scan line on the surface, and (b) element composition change along scan line.

Fig.8. EDS mapping results of oxygen elements after isothermal heat treatment at 1180ºC of (a) 1 h annealing, (b) 10 h annealing, (c) 50 h annealing, (d) 100 h annealing and at 1480 ℃ of (e) 1 h annealing, (f) 10 h annealing, (g) 50 h annealing, (h) 100 h annealing, respectively.

Fig.9. Martens hardness results of cross-sectional top coatings, indicating that the hardness of the top coatings improved as the heat treatment times increased.

Fig.10. Young's modulus results of cross-sectional top coatings, indicating that the hardness of the top coatings improved as the heat treatment times increased.

Figures

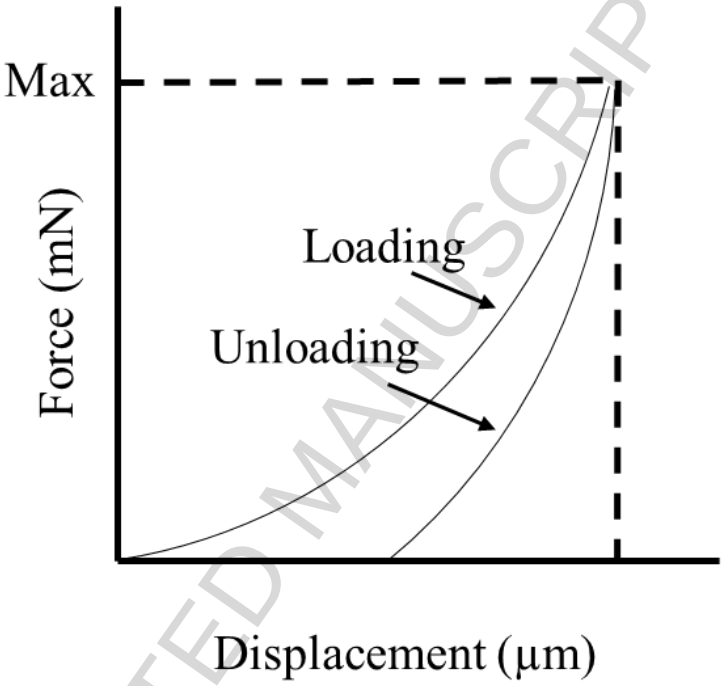

Fig.1

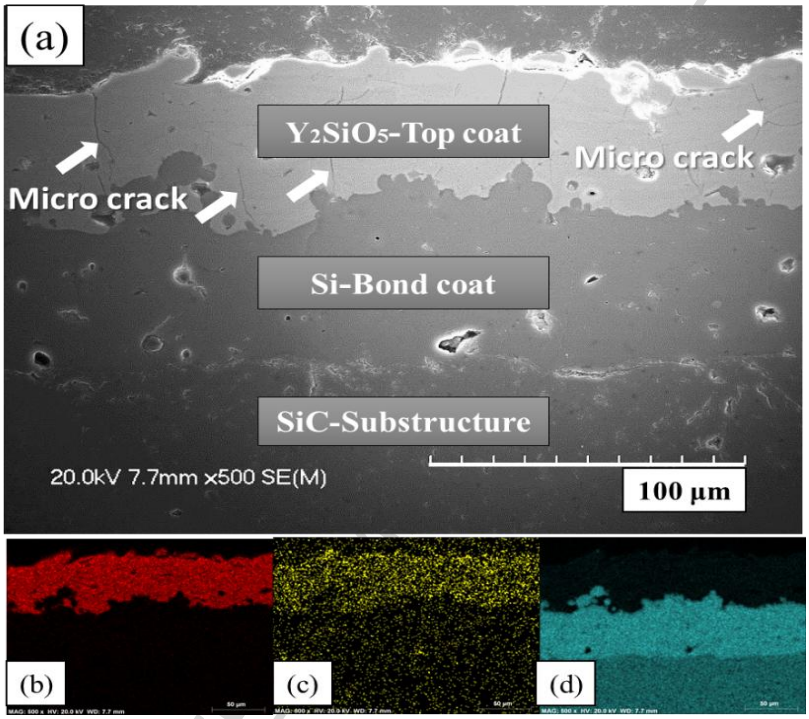

Fig.2

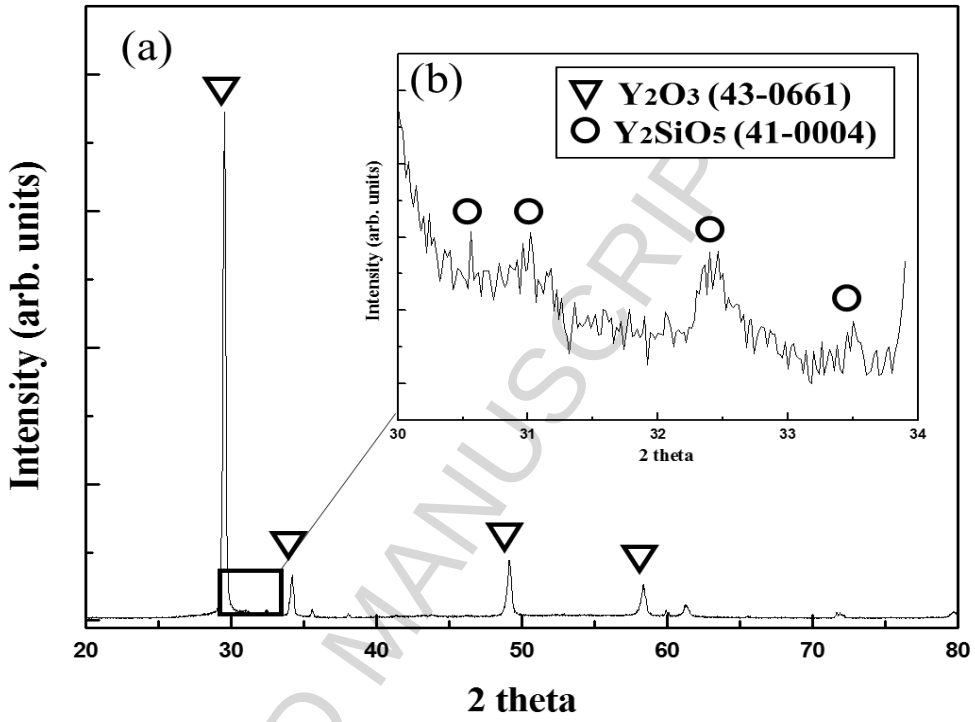

Fig.3

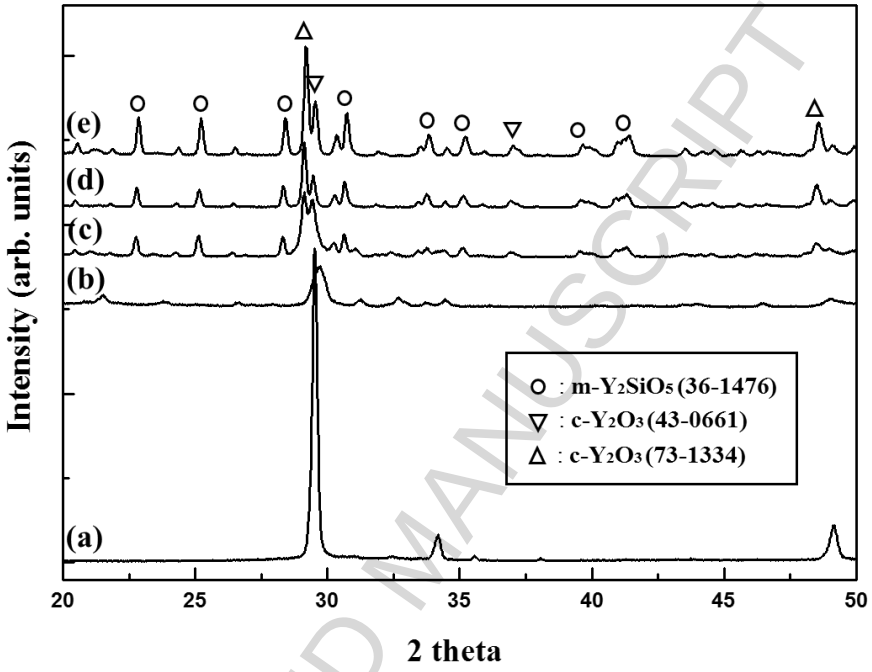

Fig.4

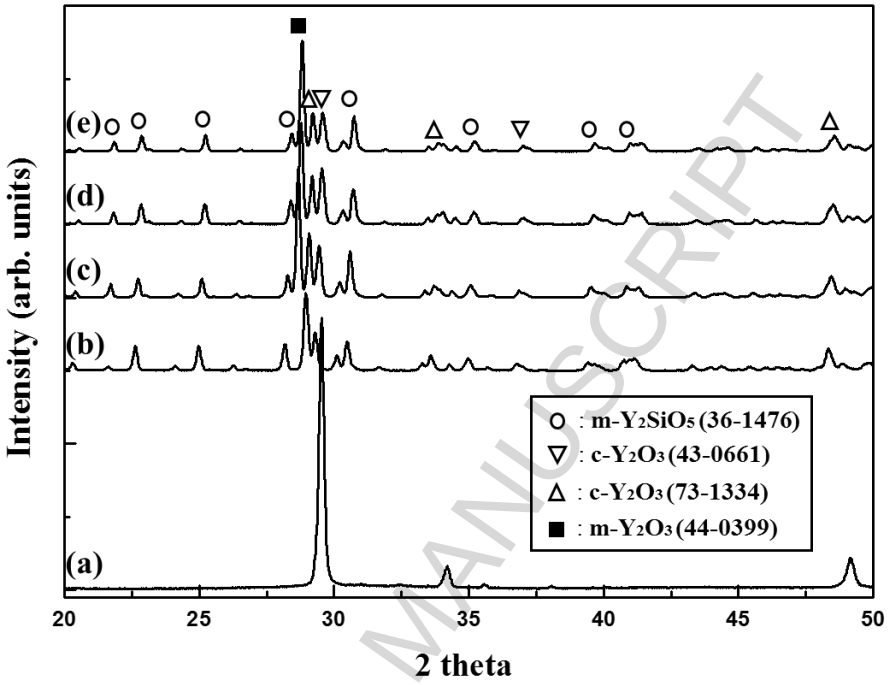

Fig.5

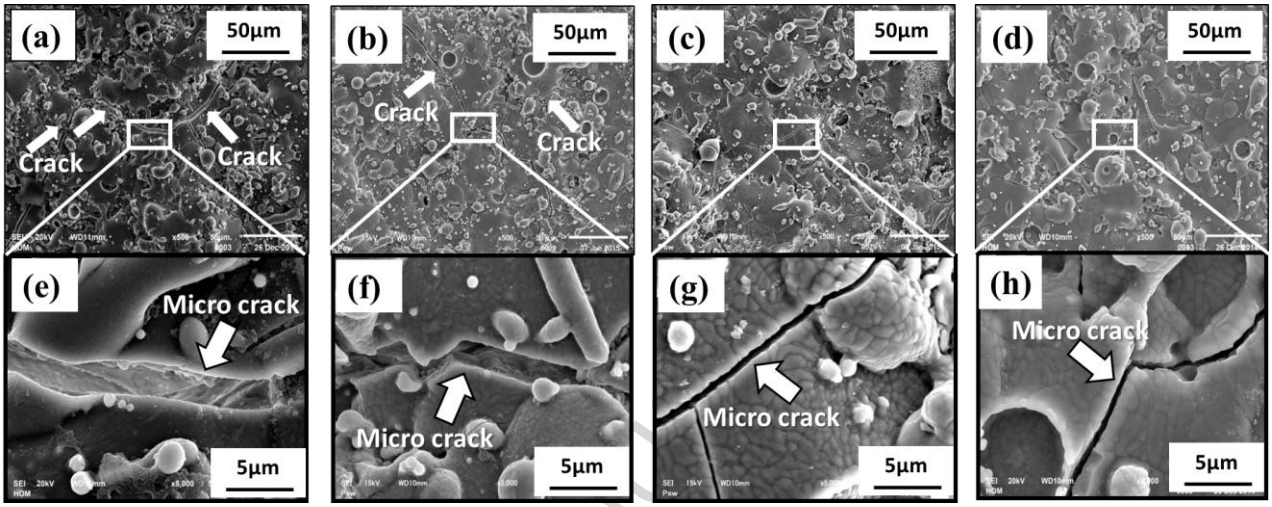

Fig.6

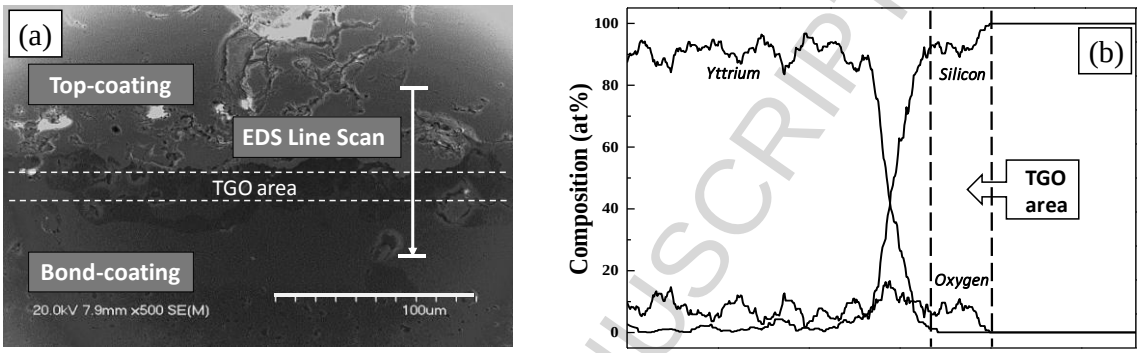

Fig.7

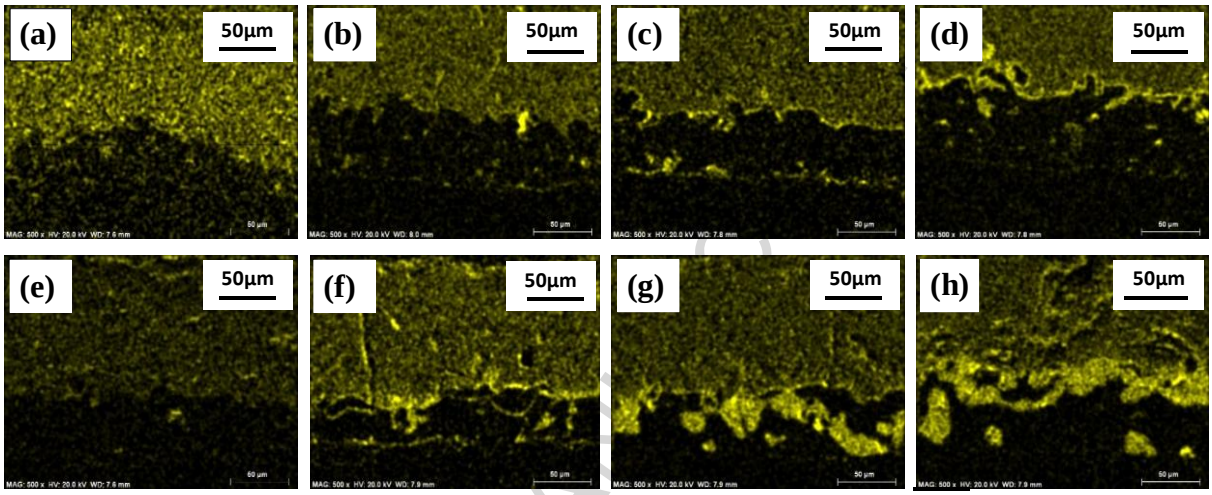

Fig.8

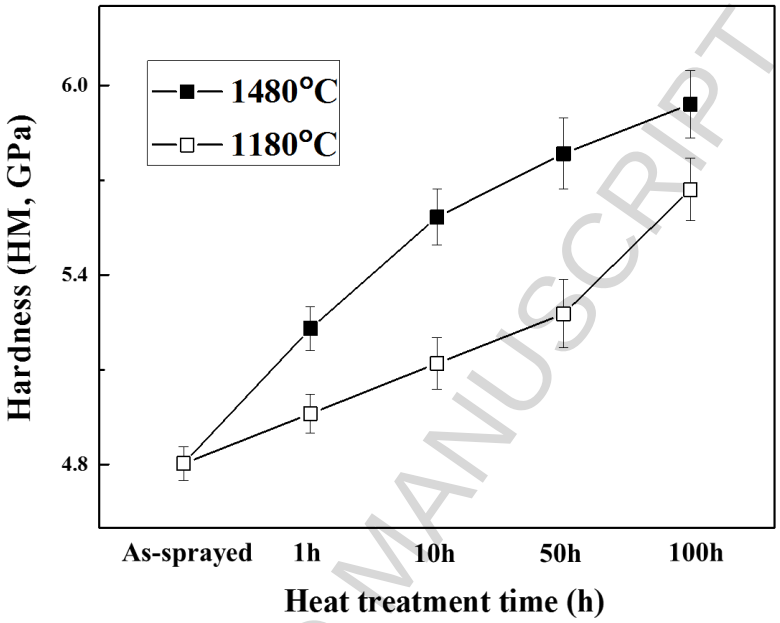

Fig.9

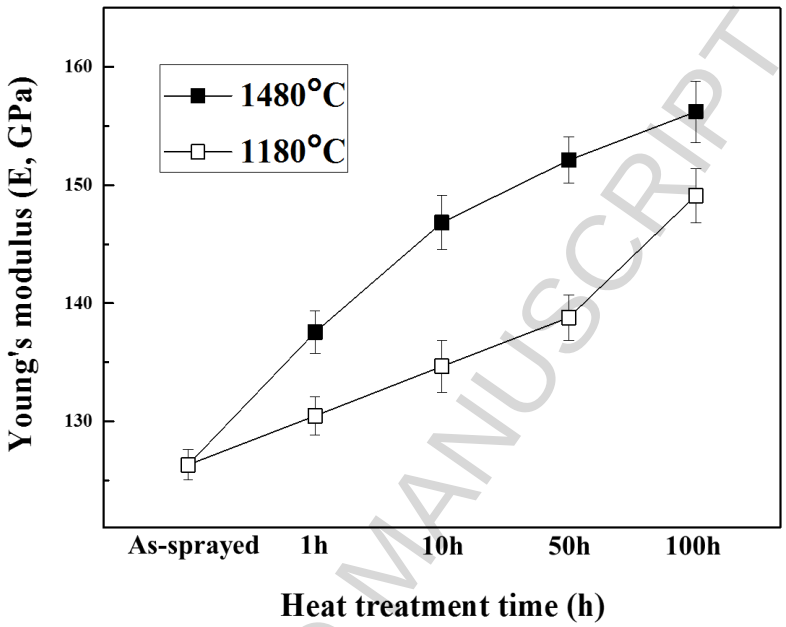

Fig.10

Highlights

- Y_2SiO_5 coatings are deposited by flame-spray technique as protection layer on SiC.
- Thermally grown oxide observed at the interface between the Y_2SiO_5 coating and Si bond coatings.
- Hardness and Young's modulus of Y_2SiO_5 coatings increased with increasing heat treatment time at 1180ºC and 1480ºC.